Water experiment for assessing vibroacoustic beamforming gain for acoustic leak detection in a sodium-heated steam generator

Souha Kassab, Frédéric Michel, Laurent Maxit

Water experiment for assessing vibroacoustic beamforming gain for acoustic leak detection in a sodium-heated steam generator

Souha Kassab [1,2], Frédéric Michel[2], Laurent Maxit[1]

1. INSA–Lyon, Laboratoire Vibrations-Acoustique (LVA), 25 bis, av. Jean Capelle, F-69621, Villeurbanne Cedex, France.

e-mail: laurent.maxit@insa-lyon.fr (corresponding author)

2. CEA, DEN,DTN/STPA/LISM, F-13115 Saint-Paul-lez-Durance, France.

Abstract: A technique based on vibration measurements has been developed to detect water leaking into sodium in view to improving the monitoring of steam generators. Leak-induced vibrations can be masked by background noise. This problem can be overcome by employing a beamforming technique to increase the signal-to-noise ratio (SNR). In order to study the feasibility and efficiency of this technique for the present configuration, experimental investigations were performed on a mock-up composed of a straight cylindrical pipe coupled to a hydraulic circuit by two flanges. A sound emitter introduced in the pipe simulates the source to be detected while the background noise vibrations are controlled by flow speed. Beamforming is applied to the signals measured by an array of accelerometers mounted externally on the pipe. Two different types of beamforming are considered: the conventional (Bartlett) type and an advanced type based on SNR maximization (MaxSNR). After analysing the vibroacoustic behaviour of the mock-up, the article focuses on the efficiency of the two beamforming treatments for narrow and broad bands.

Keywords: sodium-heated steam generator, leak detection, beamforming, array gain, structural acoustics, water pipe.

Highlights:

- A vibroacoustic leak detection system for sodium heated steam generator is studied.
- An array of accelerometers fixed on the external shell is used for detection.
- Two types of beamforming treatments are studied to increase the Signal to Noise ratio.
- A water experiment confirms the efficiency of the MaxSNR treatment.

1. Introduction

This paper describes the study of a non-intrusive vibroacoustic beamforming technique designed to detect sodium-water reactions in the steam generator unit (SGU) of a liquid sodium fast reactor (SFR). Early detection is important since sodium/water reactions can lead to severe damage if appropriate action is not taken quickly. Different works considering active [1] and passive [2] detection techniques have been carried out in the past. The passive techniques are based on the fact that the considerable differences of pressure and the strong sodium/water chemical reaction caused by the leak generate acoustic noise. Acoustic techniques can be used to detect the leak quickly as the propagation time of the acoustic wave from the leak to the sensors on the external surface of the SGU is sufficiently short. However, these methods are very sensitive to the background noise caused by the sodium and water flows, boiling water and the vibrations induced by the pumps. Kim et al. [3] studied the noise spectrum induced by the sodium-water reaction for various leak rates lower than 1 g/s. They concluded that a small leak at a rate of 0.4 to 0.6 g/s generates a wide band of 1 to 200 kHz noise that can be detected using a single sensor and a threshold criterion. For microleaks, the signal-to-noise ratio can however be lower than 0 dB, and a more complex signal processing technology may be required. Hayashi et al. [4] applied a nonlinear signal processing method called the twice-squaring method, originally developed for the acoustic detection of boiling sodium. By mixing experimental leak noises with background noises from real steam generators, they showed that the twice-squaring method can detect a leak noise with a signal-to-noise ratio as low as -20 dB. Sing and Rao [5] investigated the detection of water injected into liquid sodium by measuring the external acoustic field with microphones located far from the system. Such a system is very simple but may be easily disturbed by external acoustic sources. Chikazawa [2] proposed an acoustic leak detection system using a delay-and-sum beamformer. A sodium-reaction noise source is assumed to be localized while the background noise is uniformly distributed. The delay-and-sum beamformer provided information on the direction of the acoustic source. The numerical investigations showed that it could distinguish the source of the sodium-water reaction from the SGU background noise even if they had similar magnitudes. A water experiment with mock-up tube bundles was performed five years later [6]. A linear array of five hydrophones was immerged in a water tank and the previous numerical results were confirmed. It was also shown that the tube bundle did not modify the performance of the array for the frequencies considered (around 10 kHz). Another type of beamforming we consider in this paper is based on measuring the vibrations of the external surface of the SGU instead of measuring the pressure inside the

fluid. This vibroacoustic beamforming technique was developed in the framework of the PhD thesis of Moriot [7]. Beamforming over an array of sensors is of particular interest due to its capacity to increase the signal-to-noise ratio of the acoustic signal induced by the water-sodium reaction, generally masked by the SGU background noise, as shown by Kim et al. [3]. Moriot et al. [8] considered conventional beamforming (sometimes called Bartlett beamforming), based on knowledge of the source to be detected and by assuming that the background noise is spatially uncorrelated. In the numerical applications, the source was assumed to be an acoustic monopole (i.e. pulsating sphere). The steering vectors of the beamforming were therefore defined from the frequency transfer functions between an assumed position of the monopole source inside the detection space and the sensor mounted on the external surface of the shell. These steering vectors took account of the strong interaction between the fluid (i.e. sodium) and the cylindrical shell (i.e. external surface of the SGU). The numerical results obtained by Moriot et al. [8,9] showed that vibroacoustic beamforming using a linear array of accelerometers fixed on the external surface of the cylindrical shell can be used to localize the acoustic monopole. However, the main interest of using beamforming for detection remains the increase of the SNR. This is generally quantified by the array gain, defined as the ratio of the SNR at the beamforming output relative to the SNR at the reference sensor (i.e. the sensor exhibiting the highest SNR). Based on detection at a threshold criterion at the beamforming output (instead of the reference sensor), this gain allows improving the detection rate while limiting the sensitivity of the array to false alarms. The works of Moriot et al. [8] reported promising results in terms of array gain, both numerically and experimentally. However, the numerical results were obtained by using simple academic models (an infinite plate in [9] and an infinite cylindrical shell in Moriot et al. [8]) under the assumption of uncorrelated background noise. These assumptions, which underpinned the first investigations, were not fully satisfactory for practical application. Also, the experimental data were limited to a handful of frequencies for the harmonic acoustic source considered [7, 8].Wideband analysis could not be carried out with this type of excitation whereas the water-sodium reaction is a wideband source [3]. Moreover, it was observed that the vibratory background noise could be significantly correlated for the highest flow speeds considered. It was found that the beamforming performances could be deteriorated (i.e. decrease of the array gain). New experimental investigations are carried out in the present paper to back up the first results related to vibroacoustic beamforming [7-9]. The configuration considered for the experiment is illustrated in figure 1. It consists of the mock-up developed during Moriot's PhD study. It is composed of a cylindrical pipe filled with a fluid (i.e. water rather than sodium for practical reasons) connected to the hydraulic circuit by two

flanges. The source to be detected consists of a hydrophone used in transmission mode placed inside the pipe whereas the background noise may be controlled by changing the flow rate. The vibroacoustic beamforming consists in processing the signals of the accelerometers fixed on the pipe to enhance the source signal and reject the background noise.

This experiment will focus on three aspects that have not yet been studied and which constitute the novelty of the present paper:

- First, we analyse the beamforming performance for a large frequency range (i.e. [1 kHz-5 kHz]), considering both the conventional treatment and the MaxSNR treatment [10-11]. The latter was proposed in the past to maximize the SNR at the beamforming output based on knowledge of both the acoustic source and the background noise. It may provide advantages in comparison to the classical beamforming method, in particular in the case of partially-space correlated background noise. In the first part of the study, the beamforming analysis will be performed in narrow bands (i.e. a width of 4 Hz) from 1 kHz to 5 kHz.
- Second, we study the relations between the vibroacoustic response of the system considered and the beamforming output. The goal is in particular to identify if the resonances of the system considered influence the beamforming performances.
- Finally, wideband beamforming analysis will be carried out to conform with the fact that a wideband source should be detected for practical applications [3].

In addition to these three aspects, we demonstrate in particular that the MaxSNR beamforming treatment significantly increases the SNR for the pipe system considered, despite the presence of resonances of the pipe and a partially correlated background noise.

The paper is organized as follows:

- Section 2 recalls the principle of classical and MaxSNR beamforming as well as the definition of the array gain;
- Section 3 presents the experimental set-up;
- The vibroacoustic characteristics of the mock-up are studied in section 4;
- The beamforming performances are analysed in section 5.
- Section 6 summarises the main findings on the water experiment and provides a discussion on their generalisabilities in the SGU application.

2. Classical and MaxSNR beamforming treatments

In this section, we recall the principles of classical and MaxSNR beamforming treatments [10] and define the different quantities considered. These principles and definitions are given for the case presented in the introduction and in figure 1.

The cross-spectral matrix at the angular frequency ω of the signals received by the accelerometers composing the array fixed on the pipe are denoted $\Gamma(\omega)$. If the array is composed of *n* accelerometers, Γ is a square matrix of dimensions $n \times n$ and the component of the raw *#i* and the column *#j* corresponds to the cross-spectrum density (CSD) function of the signals of sensors *#i* and *#j at frequency* ω, $S_{ij}(\omega)$:

$$\Gamma(\omega) = \left[S_{ij}(\omega)\right]_{n\times n} \quad (1)$$

Assuming that the signals induced by the source to be detected and the signals of the background noise are independent, matrix Γ can be decomposed such that:

$$\Gamma = \Gamma^s + \Gamma^n\,, \quad (2)$$

where Γ^s is the cross-spectral matrix of the signals induced by the source alone and Γ^n is the cross-spectral matrix of the signals induced by the background noise alone.

Beamforming consists of a 'spatial' filter of the signals received by the array of sensors. We define the pre-filtering state before presenting this filter. It corresponds to the analysis of each sensor's signal independently. The SNR of the sensor *#i* is then given by:

$$\mathrm{SNR}_i(\omega) = 10\log_{10}\left(\frac{S_{ii}^s(\omega)}{S_{ii}^n(\omega)}\right), \quad (3)$$

where S_{ii}^s is the auto-spectral density (ASD) function of the signal measured by sensor *#i* in the presence of the source alone and S_{ii}^n is the ASD function of the signal measured by sensor *#i* in the presence the background noise alone.

Without beamforming, acoustic leak detection can be based on applying a threshold criterion to the signals received by each sensor, independently. As the vibrations induced by the source and by the background noise are not necessary uniformly distributed on the pipe, the SNR may vary from one sensor to another. For a given position of the source, the sensor having the highest SNR is therefore the most appropriate obtained by detection with the threshold criterion. To define the 'best' pre-filtering state, we define the reference sensor at angular frequency ω as

the sensor having the highest SNR at this frequency. The reference $\mathrm{SNR}^{\mathrm{ref}}$ is therefore the SNR of the reference sensor:

$$\mathrm{SNR}^{\mathrm{ref}}(\omega) = \max_{i\in[1,n]}[\mathrm{SNR}_i(\omega)] \tag{4}$$

The beamforming treatment is defined after having defined the pre-filtering state. The spatial filter of this treatment is characterized by the so-called steering vector F_u, which will be defined for each position u of the detection space. The latter represents the possible positions of the source to be detected. For the present configuration (see figure 1), the detection space consists of the fluid volume inside the pipe. The beamforming output at position u, y_u is given by [8]:

$$y_u(\omega) = F_u^*(\omega)\Gamma(\omega)F_u(\omega), \tag{5}$$

where the asterisk denotes the Hermitian conjugate.

The SNR at the beamforming output is then defined by:

$$SNR^{BF}(\omega) = 10\log_{10}\left(\frac{y_s^s(\omega)}{y_s^n(\omega)}\right) = 10\log_{10}\left(\frac{F_s^*(\omega)\Gamma^s(\omega)F_s(\omega)}{F_s^*(\omega)\Gamma^n(\omega)F_s(\omega)}\right), \tag{6}$$

where y_s^s is the output of the beamforming steering at the position of the source in the presence of the source only, and y_s^n is the output of the beamforming steering at the position of the source in the presence of the noise only.

The main interest of beamforming for detection is that the SNR at the beamforming output is significantly higher than the SNR at the reference sensor. It is then possible to define the array gain, $G(\omega)$ by (recalling that the SNR quantities are defined in dB):

$$G(\omega) = SNR^{BF}(\omega) - \mathrm{SNR}^{\mathrm{ref}}(\omega) \tag{7}$$

Up to now, the steering vectors, F_u have not been defined. Various definitions have been proposed in the literature [11] as a function of different purposes (for instance, localisation and detection) and of prior knowledge of different quantities. Two definitions are considered: one related to conventional beamforming as used by Moriot et al. [8], and MaxSNR beamforming ([10-11]) that focuses on maximizing the SNR at the beamforming output.

• **Conventional beamforming**

For this treatment, it is assumed that the source to be detected is characterized by the transfer functions between the source at any position u in the detection space and the vibrations measured at the n sensor positions. The vector containing these transfer functions for a given position u of the source is denoted $\mathrm{H}_u(\omega) = \left[H_{u,i}(\omega)\right]_{n\times 1}$. More precisely, the transfer function between the position u of the source and the sensor #i, $H_{u,i}(\omega)$ is defined as the ratio of the acceleration measured at sensor #i over the source strength (i.e. volume velocity). There are two approaches for estimating these transfer functions: the first consists in assuming that the source can be represented by an acoustic monopole and by using an accurate vibroacoustic model of the system considered ([7, 8]). However, it was shown in [8] that simple models like a fluid filled cylindrical shell model are not sufficiently accurate to represent these transfer functions for beamforming applications. Efforts will be made in the future to develop more accurate numerical models. The second approach considered in the present paper consists in measuring these transfer functions directly. This avoids the issues of reliability raised by the numerical model but requires that source is moved inside the detection space.

Considering the transfer functions, the cross-spectral matrix of the signals induced by the source Γ^s can be rewritten $\Gamma^s = q_s(\omega)\mathrm{H}_s(\omega)\mathrm{H}_s{}^*(\omega)$ where $q_s(\omega)$ characterizes the strength of the source.

Regarding the background noise, it is assumed that it is spatially homogeneous and incoherent. The cross-spectral matrix of the accelerations in the presence of the background noise alone can be written $\Gamma^n = \sigma_n(\omega)\mathrm{I}$ where I is the identity matrix and σ_n is the ASD function of the background noise acceleration. Under these assumptions and considering Eqs. (2) and (5), the beamforming output at position u can be rewritten: $y_u(\omega) = q_s(\omega)|\mathrm{H}_s(\omega)F_u^*(\omega)|^2 + \sigma_n(\omega)F_u^*(\omega)F_u(\omega)$.

In conventional beamforming, the steering vector is chosen such that the beamforming output, y_u is maximum when the beamforming focuses on the position of the source (i.e. u=s). To avoid the solution $\|F_u\| \to \infty$, it is commonly assumed [12-14] that $\|F_u\| = 1$ where $\|\ \|$ represents the Euclidean norm. The quantity $|\mathrm{H}_s(\omega)F_u^*(\omega)|$ that remains to be maximized can be seen as the scalar product between the vectors H_s and F_u^*. Thanks to the Cauchy-Schwarz inequality, the maximum is obtained when the two vectors are collinear. As $\|F_u\| = 1$, we obtain:

$$F_u^{class}(\omega) = \frac{H_u(\omega)}{\|H_u(\omega)\|}. \quad (8)$$

This definition of the steering vector ensures that this treatment is well adapted for localizing the source in the detection space. It relies on prior knowledge of the source (i.e. through the transfer functions H_u) and on the assumption of spatially uncorrelated background noise. It is commonly applied in many industrial applications for detecting plane wave sources in free space (i.e. submarines, radar, etc). In the following, it is referred to as "conventional" beamforming treatment.

- **MaxSNR beamforming**

In some situations (as observed by Moriot [7, 8] for significant flow speeds), the background noises measured at the different sensors can be partially correlated. This means that the assumption of the classical beamforming is violated, inevitably leading to a decrease in beamforming performance.

To overcome this obstacle, different variants of beamforming based on prior knowledge of the background noise (as well as of the source) were developed [11]. In particular, the so called "MaxSNR" beamforming was developed to maximize the SNR at the beamforming output. The optimal steering vector is therefore defined as follows:

$$F_u^{opt}(\omega) = \underset{F_u}{\operatorname{argmax}} \left[\frac{F_u^*(\omega)\Gamma_u^s(\omega)F_u(\omega)}{F_u^*(\omega)\Gamma^n(\omega)F_u(\omega)} \right]. \quad (8)$$

This definition requires knowledge of the cross-spectral matrix related to the background noise, Γ^n. It can be estimated experimentally from different *in situ* measurements performed at different times for which it can be assumed that the source is not active (i.e. periods without leaks). It can also be regularly re-estimated to take variations of the background noise into account. Definition (8) also requires an evaluation of Γ_u^s, the cross-spectral matrix of the signals induced by the source located at a given position *u* in the detection space. This quantity can be written:

$$\Gamma_u^s(\omega) = \sigma_s(\omega)H_u(\omega){H_u}^*(\omega)\,, \quad (9)$$

where σ_s is the ASD function of the source strength.

By injecting Eq. (9) in Eq. (8), we obtain:

$$F_u^{opt}(\omega) = \underset{F_u}{\operatorname{argmax}} \left[\frac{F_u^*(\omega) H_u(\omega) H_u{}^*(\omega) F_u(\omega)}{F_u^*(\omega) \Gamma^n(\omega) F_u(\omega)} \right]. \quad (10)$$

The mathematical problem then depends on H_u and Γ^n. From bilinear algebra considerations [10], it can be shown that the solution of Eq. (10) corresponds to one eigenvector associated with the largest eigenvalue of the matrix $(\Gamma^n)^{-1} H_u H_u^*$:

$$(\Gamma^n)^{-1} H_u H_u^* F_u^{opt} = \lambda_{max} F_u^{opt}. \quad (11)$$

The beamforming treatment considering these optimized steering vectors F_u^{opt} allows us to theoretically maximize the signal-to-noise ratio at the output of beamforming. However, the technique requires solving a generalized eigenvalue problem which can be time consuming. Compared to classical beamforming, it also requires knowledge of the noise cross-spectral matrix.

3. Presentation of the experimental mock-up

The experimental set-up used to evaluate the performance of vibroacoustic beamforming for detecting an acoustic source in a fluid is illustrated in Figure 2 whereas the instrumentation used for the signal processing is summarized in Table 1.

Device	**Purpose of Use**
Hydrophone *B&K 8103* (used as a projector) [15]	Acoustic emission inside the mock-up (i.e. source to be detected)
Power amplifier *B&K 2713* [15]	Amplification of the input hydrophone signal
Generator module *B&K 3160-B-4/2*	Generator channel for the hydrophone signal
(24) Piezoelectric accelerometers *KISTLER 8704B50* [16]	Measurements of the pipe vibrations
Input module *B&K 3050-B-6/0*	Signal acquisition of the accelerometer signals
Software *Pulse B&K*	Signal generator (for the hydrophone) and data analysis (of the accelerometer signals)

Table 1. Summary of the devices used for the signal processing.

For this laboratory experiment, the steam generator shell is represented by a cylindrical pipe made of stainless steel. The length, diameter and thickness are 3.1 m, 219 mm and 8 mm, respectively. To ensure ease of implementation and safety, the fluid used inside the pipe was

water (rather than sodium) at room temperature and at a pressure of about 4 bar. The test section was connected to the hydraulic circuit by two stiff flanges. Particular attention was paid to uncouple the test section from external mechanical sources (by fixing the pipe with rubber seals on a suspended slab) and from external fluid sources (using acoustic decoupling balloons). Upstream of the test section, a 4 m long pipe and a perforated plate flow conditioner (see figure 2c) were used to stabilize the turbulent flow while a 1.5m long pipe was used for the discharge before the acoustic balloon (see figure 2a).

Nine holes were perforated in the cylindrical generator $\theta_s = 0°$ of the test pipe (see figure 2b). These holes were used to introduce the acoustic source inside the pipe at different axial positions. The acoustic source consisted of a *B&K 8103* hydrophone used in transmission mode (i.e. emitter mode). The driving signal generated by a *B&K PULSE* system was amplified by a *B&K Power Amplifier 2713*. The hydrophone was mounted on a mechanical device (see figure 2b) designed to control the radial positions of the hydrophone.

The pipe vibrations were measured by an array of 24 *KISTLER 8704B50* accelerometers fixed on the cylindrical generator $\theta_i = 90°$ (see figure 3). The spacing between the sensors was $\Delta x = 4$ cm and the first accelerometer was positioned 15 cm from the upstream flange of the flow. The axial position of the accelerometer #*i* was therefore $x_i = 0.15 + 0.04(i-1)$ for $i \in \{1,..,24\}$. The accelerometer signals were processed using the *B&K PULSE* system to extract the cross-spectral matrices, Γ. The sampling frequency and the frequency resolution were set to 16384 Hz and 4 Hz, respectively. The cross-spectral matrices were exported in order to achieve the beamforming treatments with MATLAB.

We underline that the hydrophone was small compared to the diameter of the pipe and the acoustic wavelength for the frequency band considered (i.e. up to 5 kHz). This characteristic ensured that it was well adapted for simulating a monopole source. However, the downside of this small size was the projector's poor acoustic radiation efficiency in the frequency band considered. Below 1 kHz, the signal-to-noise ratio is clearly insufficient for exploiting the results given by the accelerometers fixed on the pipe.

This experimental set-up allowed us to perform measurements for different positions of the acoustic source (i.e. hydrophone) and different flow speeds. However, for the sake of conciseness, we present only the results for the highest flow speed considered which corresponds to a flow rate of $Q_w = 140\ \mathrm{l.s^{-1}}$.

4. Analysis of the vibroacoustic response of the test section

Before studying the performances of the vibroacoustic beamforming, the vibratory response of the test section for three different excitations was analysed:

- A radial point force applied on the pipe to exhibit and highlight some vibration characteristics of the test section;
- An acoustic source inside the fluid to analyse the vibrations induced by the source to be detected;
- The pressure fluctuations induced by the turbulent flow to characterize the vibratory background noise measured by the array of accelerometers.

4.1 Radial mechanical point excitation

In order to highlight several characteristics of the vibratory field of the system considered, we first study the response of the pipe when it is excited by a radial point force. As the excitation is directly applied on the pipe, the structural waves are significantly excited and the pipe characteristics are clearly exacerbated. In the next two subsections, we will study how these pipe characteristics play a role in the distribution of spatial vibration when the pipe is excited by the source to be detected and by the turbulent flow leading to the background noise. From the practical viewpoint, these measurements with a mechanical force are not necessary for applying the beamforming as considered in the present paper. However, we underline that this type of measurement with a mechanical force on the outer hull of an SGU can be easily achieved in practice and can be used as input data for updating a vibroacoustic model of the system considered. In other words, it can be used to develop a reliable model that could then be used to predict the transfer functions between the position of the detection space and the array sensors (i.e. to evaluate the transfer functions H_u used in the definition of the steering vectors). However, this work is outside the scope of the present paper.

Figure 4 shows the vibratory field measured by the array of accelerometers for a radial mechanical excitation (i.e. impact hammer) applied at x = 0.14 m. The measurements were carried out when the pipe was filled with water at a pressure of 4 bar with the water at rest. Peaks of resonances can be observed on the FRF of the accelerometer #21 (figure 4a). They can be attributed to two physical phenomena:

- The first is related to the wave guide behaviour of the pipe filled with fluid and its capacity to exhibit propagative vibroacoustic waves in the axial direction [17-18]. For each

circumferential order *n* of the cylindrical shell (i.e. each order of a Fourier series decomposition of the vibratory field), a cut-on frequency can be defined. For frequencies below this frequency, the waves related to this circumferential order are evanescent. They do not contribute significantly to the vibratory field on the pipe. On the contrary, for frequencies above the cut-on frequency, the waves are propagative and can contribute significantly to the vibratory field. An estimation of these cut-on frequencies can be obtained by resolving the dispersion curves of an infinite fluid loaded cylindrical shell model [17-18]. The calculation was carried out for the present case considering a Young modulus of 1.85×10^{11} Pa, a mass density of 7800 kg/m^3, a Poisson coefficient of 0.3 for steel, a sound velocity of 1500 m/s, and a mass density of 1000 kg/ m^3 for water. The following cut-on frequencies were obtained: 363 Hz for *n*=2, 1079 Hz for *n*=3, 2145 Hz for *n*=4 and 3549 Hz for *n*=5;

- The second phenomenon is related to the wave reflections on the flanges. Indeed, the size of the flange section is 40 mm in the axial direction and 60 mm in the radial direction. The flanges are therefore significantly stiffer than the cylindrical shell. The mechanical impedance mismatch at the interface between the pipe and the flange leads to wave reflexions at both flanges. The constructive interferences of these waves for some frequencies leads to a resonance phenomenon. In the following, these resonances are referred to as "pseudo axial modes". Strictly speaking they cannot be called "modes" as part of the energy of the vibroacoustic waves can be transmitted through the fluid (i.e. water), which is not bounded in the axial direction.

These two phenomena are closely related. Consequently, the pseudo axial modes for a given circumferential order *n* occur only for frequencies above the cut-on frequency of the circumferential order. Moreover, as the celerity in the axial direction of a propagative wave is infinite at the cut-on frequency and decreases as a function of the frequency (see the dispersion curves in [17], the result is that the density of pseudo-modes is high just above the cut-on frequency and then decreases when the frequency increases. This behaviour can be clearly observed in figure 4a. In particular, it shows the densification of peaks around 1100 Hz and 2200 Hz which are around the calculated cut-on frequencies for *n*=3 and *n*=4, respectively.

The spatial distribution of the pipe vibration measured by the array of accelerometers is shown in figure 4b. For the sake of clarity, we have plotted the shell displacements instead of the shell accelerations. Patterns with pseudo vibration nodes and antinodes can be observed at the pseudo-mode frequencies. The number of antinodes is related to the axial celerity of the vibroacoustic waves. As the celerity decreases with frequency, the wavelength also decreases

after which the number of antinodes increases with frequency. It should, however, be kept in mind that several circumferential orders can contribute at a given frequency (as soon as their cut-on frequencies are below this frequency). This may explain why the pseudo-mode at 1244 Hz has 4 antinodes on the instrumented section whereas that at 1266 Hz has only 3 antinodes. These two pseudo-modes are not related to the same circumferential order. The first is certainly related to n=2 whereas the second is related to n=3. The circumferential order of each pseudo-mode can only be confirmed by performing measurements along the circumference of the pipe, though this is outside the scope of the paper.

4.2 Acoustic source

Now, let us focus on the vibratory response of the test section when it is excited by the hydrophone used in emitter mode. A sine sweep from 500 Hz to 5 kHz was used as the input signal of the amplifier of the hydrophone. Below 1 kHz, the SNR is too low to exploit the measurements correctly, thus the results will not be shown below this frequency. Figure 5 shows the displacement results for two radial positions of the source: r_s=0.052 m and r_s =0.088 m, both for an axial position of x_s=0.56 m corresponding to the middle of the array.

As expected, it can be seen that the levels are generally significantly higher when the source is closer to the steel shell (i.e. r_s =0.088 m). Moreover, the patterns appearing in figure 5 are similar to those of figure 4 although not identical. This can be explained by the fact that the acoustic source does not excite the same pseudo axial modes as the mechanical force considered in figure 4. The radial position of the source also influences the response of the pseudo axial modes. For instance, for a source located on the axis of revolution of the shell (i.e. r_s =0 m), only the pseudo axial modes corresponding to the circumferential order n=0 are excited as in this case the system is fully axisymmetric. The further the source is from the axis of revolution, the more the circumferential orders participate in the shell response. This can be observed in figure 5, where the peak levels are globally lower above 2300 Hz than below this frequency when r_s=0.052, where they are roughly the same for the entire spectrum when r_s =0.088 m. This can be explained by a lower contribution of the circumferential order n=4 for r_s=0.052 than for r_s =0.088 m.

Finally, we recall that these transfer functions between the source and the accelerometers have been encapsulated in the vector noted $\mathrm{H}_u(\omega)$ in section 2. These transfer functions will be used for the calculation of the steering vector (with Eq. (8) for the conventional beamforming and

with Eq. (11) for the MaxSNR beamforming). The array gain will also be evaluated using these transfer functions by Eq. (9) to evaluate the cross-spectral matrix related to the source.

4.3 Turbulent flow

In the presence of the fluid at rest (only the booster pump in operation), the signals between the different accelerometers are incoherent (result not shown). However, as has already been observed by Moriot et al [8], when the flow rate increases the signals become coherent for certain frequencies (see figure 10 in [8]). However, the study by Moriot is limited to specific frequencies spaced by 1 kHz.

Figure 6 shows the normalized CSD function between sensor #1 and the other sensors for a flow rate of $140\,\mathrm{l.s^{-s}}$ and for the frequency band [1 kHz- 3 kHz]. It can be seen that the accelerometer signals are highly coherent for frequencies corresponding to pseudo axial modes (by comparing figure 5 with figure 3). This result was not expected at first sight. Instead, if the well-known model of Corcos [19] of the wall pressure field induced by a turbulent boundary layer is considered, a coherent length of the pressure field in the streamwise direction can be calculated. The latter varies from 4.1×10^{-4} m (at 3 kHz) to 1.3×10^{-3} m (at 1 kHz). As it is of almost one order of magnitude lower than the sensor spacing, the coherence of the accelerometer signals could be expected to be weak. Finally, it appears that this is not the case as the system considered reacts to this weakly correlated excitation. The result is that the vibratory response is strongly correlated (in space) for the frequencies corresponding to pseudo axial modes. This explanation was confirmed by numerical investigations considering an infinite shell model coupled to two ring stiffeners and excited by a homogenous established TBL excitation [20]. This strong coherence of the vibratory field at certain frequencies is clearly a drawback for the conventional beamforming which assumes that the background noise is uncorrelated. It is however necessary to establish the performance of this treatment in this particular condition for both narrow and wide band analysis. This strong coherence of the background noise also led us to consider another type of treatment, i.e. the MaxSNR beamforming introduced previously. For this treatment, based on prior knowledge of the background noise, it must be emphasised that the measurements performed for this flow rate (without the acoustic source) gives us the cross-spectral matrix of the background noise, Γ^n used in Eq. (11) to estimate the steering vector.

5. Analysis of beamforming performances

In the previous section, we analysed the accelerometer signals induced by the source to be detected (i.e. section 4.2) as well as those induced by the turbulent flow which represent the background noise (i.e. section 4.3). These quantities are used to evaluate both the steering vectors and the performance of the beamforming. We underline that this case represents an ideal case. However, in practice for the detection on the SGU, the vibrations induced by the source or those of the background noise can vary as a function of time, depending on the functional state of the installation. The values of the quantities used for estimating the steering vectors at an initial time are thus not necessarily representative of the values of the same quantities at the time of detection. Here, we do not study the effect of these time variations of the signals induced by the source or of the background noise which may be due to many parameters related to the practical application.

5.1 Narrow band analysis

As was described in section 2, a pre-filtering state is defined by the reference sensor and the reference SNR. This information is given in figure 7 for an acoustic source located at $(x_s, r_s) = (0.56\ \text{m}, 0.052\ \text{m})$ and a flow rate of 140 l/s. It can be seen that the reference sensor varies from one frequency to another in the frequency band [1 kHz-5 kHz] studied. This results from the variation with frequency of the spatial distribution of the vibratory field induced by the source (as shown on figure 5) as well as the variations induced by the turbulent flow. The SNR of the reference sensor increases globally as a function of the frequency. This is mainly due to a decrease of the background noise with frequency. It is noteworthy that this definition of the SNR of the reference sensor is only valid for narrow band analysis. The SNR of the reference sensor for wide band analysis will be defined in section 2.

Figure 8 shows the levels of the beamforming output for the acoustic source 'only' (i.e. source with a very low background noise when the fluid is at rest) and for the background noise due to the turbulent flow at a flow rate of 140 l/s. These results were obtained when the beamforming focuses on the source using Eq. (8) with the steering vectors evaluated as described previously. Figure 8a corresponds to the conventional beamforming whereas figure 8b corresponds to the MaxSNR beamforming. The levels are expressed in dB with the same range on the two graphs. It can be seen that the levels of the MaxSNR beamforming are always lower than those of the conventional beamforming whatever the frequency. The differences between the two techniques appear larger for the treatment of the background noise than for the

signals due to the acoustic source. This highlights the capacity of the MaxSNR beamforming to reject the background noise. The result is that the SNR at the beamforming output (i.e. difference between the output level with the source and with the background noise, see Eq. (6)) is generally larger for the MaxSNR beamforming than for the conventional one. The SNR at the beamforming output can be compared with the SNR of reference sensor by focusing on the array gain defined by Eq. (7). The result is shown in figure 9. The gain of the MaxSNR beamforming is clearly significantly larger than that of the conventional beamforming whatever the frequency inside the frequency range studied. This results directly from the definition of the steering vectors of the MaxSNR beamforming, which maximize the SNR at the beamforming output, whereas the conventional beamforming assumes an uncorrelated background noise. The gain of the conventional beamforming exhibits significant values (i.e. 5-7 dB) at certain specific frequencies but relatively low values in general. It can even be negative. These poor performances may be related to the strong coherence of the vibratory field induced by the turbulent flow, as observed in figure 6 for the frequencies corresponding to the pseudo axial modes. To confirm this statement, we evaluated the gain of the conventional beamforming using a homogeneous uncorrelated background noise instead of using the signals measured on the test section. The result is plotted with a dotted line in figure 9. For this theoretical case, the figure shows a gain varying around 9 dB, always significantly larger than that obtained with the background noise measured. This confirms the strong negative influence of the background noise coherence on the conventional beamforming performance for the present case. For some frequencies (for instance, above 4.5 kHz), these theoretical gains of the conventional beamforming may be lower than those of the MaxSNR beamforming. In some situations, knowledge of the background noise permits obtaining significant gain that cannot be obtained without this knowledge, even in the idealized case (i.e. uncorrelated background noise).

The analysis of the vibroacoustic behaviour of the test section in section 4 showed the influence of pseudo-axial modes on the vibratory response of the pipe. Resonant peaks can be observed on the vibratory spectrum when the test section is excited by, either, the acoustic source to be detected or the turbulent flow inducing the background noise. In order to study the influence of these resonances on the beamforming performances, the values of the array gain for the two types of beamforming are given in Table 2 for the resonant frequencies identified from the FRF of figure 4a. These values should be compared to the values given in figure 9 for the whole frequency range. Moreover, the values corresponding to local peaks on the curves of the gain are written in bold type in Table 2. It can be seen that the array gains are not necessarily higher

or lower for the resonant frequencies compared to the other (non-resonant) frequencies. Moreover, at certain resonant frequencies (for instance 1216 Hz), the curve of the gain can exhibit a local peak whereas at other resonant frequencies (for instance 1244 Hz), this is not the case. On the one hand, it may be due to the fact that the acoustic source does not significantly excite certain modes in comparison to others (see figure 5a); and on the other hand, it may be due to the spatial coherence of the background noise that varies from one resonant frequency to another (see figure 6).

Frequency (Hz)	1068	1096	1132	1164	1216	1244	1260	1336	1416	1512
Conv. Gain (dB)	-5.1	**-1.2**	-4.7	-2.6	**-1.1**	-5.8	-3.6	-4.0	-1.2	-3.2
MaxSNR Gain (dB)	11.4	**12.7**	8.5	11.1	**15.3**	6.8	**15.3**	8.0	**7.4**	9.5

Frequency (Hz)	1616	1728	1848	1976	2112	2244	2368	2428	2496	2564
Conv. Gain (dB)	-0.8	-1.8	-2.6	-8.8	-1.2	-2.7	**2.1**	-2.1	-0.6	0.2
MaxSNR Gain (dB)	4.4	6.8	**10.7**	6.6	**10.1**	7.8	9.4	6.1	2.8	3

Table 2. Gain values for resonance frequencies identified in figure 4a. Case of an acoustic source at $(x_s, r_s, \theta_s) = (0.56\text{ m}, 0.052\text{ m}, 0°)$ and for a flow rate of 140 l/s. Bold values indicate local peaks on the gain curve.

5.2 Wide band analysis

In practice, the source to be detected (i.e. water-sodium reaction) is a broadband excitation (Kim et al. 2010). Thus, it may be relevant to utilize all the energy induced by the source in a wide band instead of focusing on a single frequency, such as for narrow band analysis.

A wide band analysis on a given signal consists in estimating the time-average of the square signal after filtering with a band pass filter $[\omega_1, \omega_2]$. This quantity can be estimated with the ASD function of the signal and by integrating it in the frequency band $[\omega_1, \omega_2]$. It is then possible to define the SNR in the band $[\omega_1, \omega_2]$ for each accelerometer *i* by:

$$\mathrm{SNR}_i[\omega_1, \omega_2] = 10\log_{10}\left(\frac{\int_{\omega_1}^{\omega_2} S_{ii}^s(\omega)d\omega}{\int_{\omega_1}^{\omega_2} S_{ii}^n(\omega)d\omega}\right). \quad (12)$$

The reference sensor for the band $[\omega_1, \omega_2]$ is defined as the sensor having the highest SNR in this band. The SNR of the reference sensor in the band $[\omega_1, \omega_2]$ is therefore:

$$\mathrm{SNR}^{\mathrm{ref}}[\omega_1, \omega_2] = \max_{i \in [1,n]} \left[\mathrm{SNR}_i[\omega_1, \omega_2]\right]. \quad (13)$$

Figure 10 shows the values of this quantity for bands with a bandwidth of 500 Hz. The case presented is the same as in section 5.1. This figure can be compared to figure 7. It can be seen that the SNR values of the reference sensor for wide band analysis are globally lower than those of the narrow band analysis. This can be explained by the fact that the reference sensor changes from one frequency to another for narrow band analysis (as seen in figure 7a), whereas a single reference sensor is attributed to all the frequencies contained in the frequency band for wide band analysis.

The beamforming output level for the band $[\omega_1, \omega_2]$ is deduced from the numerical integration of the frequency-dependent output $y_u(\omega)$ over the frequency band $[\omega_1, \omega_2]$. The SNR can then be evaluated at the beamforming output and for the array gain for the band $[\omega_1, \omega_2]$.

Figure 11 shows the array gain obtained for bands of 500 Hz bandwidth. The array gain of the conventional beamforming remains below 5 dB (excepted for the band [2 kHz-2.5 kHz]). It appears that this treatment is inefficient for these flow conditions. In the rest of the paper, we focus on the performance of MaxSNR beamforming. For this treatment, the array gain is significant, with variations between 9 dB and 23 dB. These values appear globally higher than those observed in narrow bands. This can be attributed to both the difference of the pre-filtering reference between the two analyses (as was pointed out previously by comparing the SNR of the reference sensor of figures 7 and 10) and the integration of the beamforming output in the frequency band.

Figure 12 allows studying the variations of the gain as a function of the source positions. When the source is positioned axially at the middle of the array (i.e. $x_s = 0.56$ m), it can be seen that the gain is generally larger for $r_s = 0.088$ m than for $r_s = 0.052$ m. Compared to the latter, the first position is closer to the wall of the cylindrical shell. As discussed in section 4.2, the vibratory levels are higher for $r_s = 0.088$ m than for $r_s = 0.052$ m (see figure 5). However, this should not influence the array gain as it expresses an increase of SNR compared to the SNR of the reference sensor. It is most likely due to the fact that for frequencies above 2.3 kHz, the circumferential order n=4 is less predominant for r_s=0.052 than for r_s =0.088 m (as discussed in section 4.2) whereas it remains significant for the background noise (see figure 6). This could explain the lower gain for r_s=0.052 than for r_s =0.088 for frequency bands above 2 kHz.

On the other hand, when the source is not located in front of the array gain (i.e. for $x_s = 1.56$ m or for $x_s = 2.06$ m), it can be seen that the gain is generally slightly lower compared to the case $x_s = 0.56$ m but remains significant. This shows that the MaxSNR beamforming can be efficient even if the source is in front of the array.

The beamforming output levels in the detection space $\theta = 0°$ are shown in Figure 13 for the 4 source positions. These results correspond to the frequency band [4.5 kHz-5 kHz]. The measurements were performed for only 9 positions of the 15 positions defining the detection space. The 6 positions that are unavailable for applying the beamforming are indicated by white crosses in the figure. Figure 13a shows the output levels induced by the background noise (i.e. without the source to be detected). It is almost uniform around -43dB. The output levels in the presence of the source are shown in Figure 13b-d for the four positions. The real location of the source is symbolised by a black spot. In opposition to conventional beamforming, the steering vectors of the MaxSNR are not defined such that the beamforming output is maximum when the beamforming focuses on the position of the source. However, it can be seen that the output level is always highest in the detection space for the real position of the source. For the present case, it appears that the MaxSNR beamforming is able to localize the source. This figure allows highlighting the interest of beamforming for increasing the SNR. Indeed, the SNRs of the reference sensor are respectively, 14, 16, 17 and 11 dB for the positions of figure 13b-d. In figure 13b, for instance, the maximum output level of the MaxSNR beamforming is -7 dB whereas the output with only background noise is -43 dB (see figure 13a). The difference of 36 dB between a state without the source and with the source is 22 dB larger than the SNR of the reference sensor (i.e. 14 dB). This increase in level (corresponding to the array gain) can be used to detect the source minimizing the false alarm rate.

6. Concluding discussion

The works presented in this paper were performed in the framework of developing a non-intrusive monitoring technique for detecting a sodium-water reaction in the steam generator unit of a liquid sodium fast reactor. The technique is based on vibratory measurements on the external shell of the steam generator unit. Vibroacoustic beamforming can be used to increase the SNR in order to detect the signal due to the source when it is embedded in background noise. The study was conducted on a pipe test section in which the source to be detected consisted of a hydrophone used in emitter mode placed inside the pipe while the disturbing

noise was induced by the water turbulent flow. A linear array composed of 24 accelerometers fixed on the pipe was used for the vibratory measurements.

From the vibroacoustic viewpoint, the system considered is characterised by strong interactions between the vibration motions of the cylindrical shell and the acoustic wave propagation in the water. Moreover, the flanges used to connect the test section to the hydraulic loop induce reflections of the vibratory waves. Analysis of the vibration field of the pipe allowed us to highlight several resonance frequencies of the system considered, namely the cut-on frequencies of the circumferential modes and the frequencies of the pseudo-axial modes.

The present study showed that the conventional beamforming appeared inoperative at significant flow rates (i.e. $140\ \mathrm{l.s^{-1}}$) in the band considered [1 kHz - 5 kHz]. This resulted from the strong coherences of the vibratory signals induced by the turbulent flow, in contradiction with the assumption made by the conventional beamforming.

On the other hand, significant gains (around 10 to 25 dB) were observed using the MaxSNR beamforming for different source positions which were not necessary in front of the array. They had been obtained for a wide range of frequencies. In particular, the gain remained significant in general for the cut-on frequencies of the circumferential modes and the frequencies of the pseudo-axial modes. The efficiency of the MaxSNR beamforming was therefore not influenced by the resonant behaviour of the system considered. An analysis of the beamforming output in the detection space also showed that it can be used to localise the source for the case considered.

The most interesting finding of this experimental study concerning the steam generator application is that the MaxSNR beamforming showed its ability to significantly improve the SNR of the pipe monitored, independently of its resonance behavior and even if the background noise led to array signals that were partially correlated. However, it should be recalled that this treatment was based on the following assumptions:

(1), the signals induced by the source to be detected and by the background noise are uncorrelated (see Eq. (2));

(2), the source to be detected induces stationary and fully correlated signals. The source-sensor transfer functions should be known (see Eq. (11));

(3), the background noise should not vary as a function of time and it should be characterised by the cross-spectral matrix of accelerations measured with the sensor array.

For the experiment presented, it can be reasonably assumed that the first assumption was respected whereas it should be noted that “ideal” data were considered to fulfil the two other assumptions:

- the source-sensor transfer functions considered were measured directly on the pipe;
- the cross-spectral matrix of accelerations characterising the noise was used to both define the steering vectors and evaluate the array gain. This supposes that the background noise does not fluctuate as a function of time.

For the practical application consisting in detecting sodium-water reactions in the steam generator unit (SGU), the results obtained with the MaxSNR beamforming are encouraging as they showed that the treatment is relatively insensitive to the resonances of the mechanical system and it can deal with partially correlated background noises like that induced by the turbulent flow. Concerning the assumptions described above, it could be expected that the first assumption would be satisfied for the practical applications. Contrary to the water experiment presented in this paper, a large part of the background noise may be due to the boiling noise. The influence of the leak on this boiling noise, by reducing the mass of water available for boiling can be assumed to be negligible. Instead, the monitoring technique was developed in this paper for detecting small leaks [3]. For an order of magnitude, the rate of the leak was expected to be between 0.1 to 10 g/s whereas the rate of water in the generator unit is around 100 kg/s.

For the second assumption concerning the source to be detected, it may be difficult to measure the source-sensor transfer functions on a real SGU. It will be necessary to develop a reliable vibroacoustic model of the system considered to predict them. It will certainly be a difficult task. In order to improve the reliability of the model, certain measurements with mechanical excitations on the outer hull of the SGU could be used for updating the model. Before carrying out this work on a realistic system, a vibroacoustic model of the test section considered in the present study will be developed in the near future to study the ability of such model to reproduce accurate transfer functions for the MaxSNR beamforming applications. The measurements with the impact hammer excitation presented in section 4.1 could be reused to improve the model by resolving an inverse problem in the same way as for real SGU. Moreover, in the present study, the source to be detected was idealized as a monopole source inducing fully correlated array signals. Experimental investigations should be performed in the future tofully characterise the vibrations induced by a leak of water into the sodium.

Finally, for the background noise, a sensitivity analysis of the effect of background noise variations on beamforming performance should be performed. It should be recalled that most of the background noise in an operating steam generator is due to the combined noise of sodium flow and water evaporation. The performance of the beamforming will certainly depend on the variations of these contributions. Carrying out more representative experiments is the only means of confirming the interest of vibroacoustic beamforming using the MaxSNR approach to detect sodium-water reaction in an SGU.

Acknowledgments

This work was carried out in the framework of the LabEx CeLyA ("Centre Lyonnais d'Acoustique", ANR-10-LABX-60) and the Sodium Technology project of GEN4 program (R4G/TECNA) of the Nuclear Energy Division of CEA (CEA/DEN).

References

[1] Cavaro, M., Payan, C., Jeannot, J.P., 2013. Towards the bubble presence characterization within the SFR liquid sodium, In: Proceedings of ANIMMA International Conference, Marseille, France, vol. 1127, June.

[2] Chikazawa, Y., 2010. Acoustic leak detection system for sodium-cooled reactorsteam generators using delay-and-sum beamformer. J. Nucl. Sci. Technol. 47(1), 103–110.

[3] Kim, T., Yugay, V. S., Jeong, J., Kim, J., Kim, B., Lee, T., Lee, Y., Kim, Y., Hahn D., 2010. Acoustic Leak Detection Technology for Water/Steam Small Leaks and Microleaks Into Sodium to Protect an SFR Steam Generator. Nucl. Technol. 170, 360-369.

[4] Hayashi, K., Shinohara, Y., Watanabe, K., 1996. Acoustic detection of in-sodium water leaks using twice squaring method. Ann. Nucl. Energy 23, 1249-1259.

[5] Singh, R.K., Rao, A.R., 2011. Steam Leak Detection in Advance Reactors via Acoustics method. Nucl. Eng. Des. 241, 2448–2454.

[6] Chikazawa, Y., Yoshiuji, T., 2015. Water experiment on phased array acoustic leak detection system for sodium-heated steam generator. Nucl. Eng. Des. 289, 1-7.

[7] Moriot, J., 2013. Passive vibroacoustic detection of a water-sodium reaction using beamforming on a steam generator of a liquid sodium fast reactor, PhD thesis, INSA Lyon, France, 158 p. (in French).

[8] Moriot, J., Maxit, L., Guyader, J.L., Gastaldi, O., Périsse, J., 2015. Use of beamforming for detecting an acoustic source inside a cylindrical shell filled with a heavy fluid. Mech. Syst. Signal Process 52–53, 645–662.

[9] Moriot, J., Maxit, L., Guyader, J.L., 2012. Detection and localization of a leak in a sodium fact reactor steam generator by vibration measurements. In: Proceedings of Euronoise, Prague, Czech Republic, June.

[10] Tanaka, T., Shiono, M., 2014. Acoustic Beamforming with Maximum SNR Criterion and Efficient Generalized Eigenvector Tracking. In: Proceeding of the 15th Pacific-Rim Conference on Advances in Multimedia Information Processing, Malaysia, December.

[11] Van Veen, B., Buckley, K., 1988. Beamforming: a versatile approach to spatial filtering. IEEE ASSP magazine 5 (2), 4-24.

[12] Nascimento, V., Masiero, B., Ribeiro, F., 2018. Acoustic imaging using the kronecker array transform. In: Fernandes, R., Heloiz, V., Lopes, R., Travassos J., Casimito, C., (Eds), Signals and Images: Advances and Results in Speech, Estimation, Compression, Recognition, Filtering, and Processing, CRC Press, pp. 155- 178.

[13] Krim, M., Viberg, M., 1996. Two decades of array signal processing research. IEEE Signal Processing Magazine, 13 (4), 67-94.

[14] Coldrey, M., Viberg, M., 2006. Generalization and analysis of the conventional beamformer for localization of spatially distributed sources. In: Proceeding of the 14th European Signal Processing Conference, Florence, September.

[15] Hydrophones Types 8103, 8104, 8105, 8106: Technical Documentation, Brüel & Kjær (1992).

[16] K-Shear Accelerometers type 8702B…, 8704B…: General purpose, voltage mode accelerometers, Kistler (2008)

[17] Fuller, C. R., Fahy, F. J., 1982. Characteristics of wave propagation and energy distributions in cylindrical elastic shells filled with fluid. J. Sound Vib. 81 (4), 501–518.

[18] Fuller, C. R., 1983. The input mobility of an infinite circular cylindrical elastic shell filled with fluid. J. Sound Vib. 87 (3), 409-427.

[19] Corcos G.M., 1963. The resolution of pressure in turbulence, J. Acoust. Soc. Am. 35, 192-199.

[20] Kassab, S., 2018. Vibroacoustic beamforming for the detection of an acoustic monopole inside a thin cylindrical shell coupled to a heavy fluid: Numerical and experimental developments, PhD thesis, Université de Lyon, INSA Lyon, Villeurbanne, France, 182 p. (in French).

Figure captions

Figure 1.Schematic representation of the configuration considered for assessing the performance of the vibroacoustic beamforming.

Figure 2. Experimental setup diagrams: (a), pipe test section inserted in the hydraulic loop; (b), pipe test section with various holes for inserting the hydrophone; (c), hydrophone mounting system (left) and perforated plate conditioner (right).

Figure 3. Picture of the test pipe with the linear array of accelerometers.

Figure 4. Radial displacement response of the test pipe for a unit radial mechanical point force at x=0.105 m (hammer excitation): (a), Frequency Response Function (FRF) at point x=1 m (i.e. sensor #21); (b), Displacement versus sensor position and frequency (dB, ref. 1 m).

Figure 5. Radial displacement response as a function of the sensor position and the frequency (dB, ref. 1 m) for an acoustic source excitation (i.e. hydrophone emitter) at two positions: (a), $(x_s, r_s, \theta_s) = (0.56\ \text{m}, 0.052\ \text{m}, 0°)$; (b), $(x_s, r_s, \theta_s) = (0.56\ \text{m}, 0.088\ \text{m}, 0°)$.

Figure 6. Normalized cross spectrum density function between sensor #1 and sensor #*i*. Results as a function of the position of sensor #*i* and the frequency for a flow rate of 140 l/s.

Figure 7. (a) Signal to noise ratio for the reference sensor. (b) Identification number of the reference sensor for each frequency. Case of an acoustic source at $(x_s, r_s, \theta_s) = (0.56\ \text{m}, 0.052\ \text{m}, 0°)$ and for a flow rate of 140 l/s.

Figure 8. Output levels of the beamforming, focusing on the source in the presence of the source only (full) and for the noise only (dash): (a), Conventional BF; (b), MaxSNR BF. Case of an acoustic source at $(x_s, r_s, \theta_s) = (0.56\ \text{m}, 0.052\ \text{m}, 0°)$ and for a flow rate of 140 l/s.

Figure 9. Array gain as a function of frequency: full, MaxSNR BF; dashed, conventional BF; dashed; dotted, theoretical values for the conventional BF supposing uncorrelated noise. Case of an acoustic source at $(x_s, r_s, \theta_s) = (0.56\ \text{m}, 0.052\ \text{m}, 0°)$ and for a flow rate of 140 l/s.

Figure 10. As for figure 7 for a wide band analysis of 500 Hz bandwidth.

Figure 11. As for figure 9 for a wide band analysis of 500 Hz bandwidth.

Figure 12. Gain with the MaxSNR beamforming for different source positions: full, $(x_s, r_s) = (0.56\ \text{m}, 0.052\ \text{m})$; dash, $(x_s, r_s) = (0.56\ \text{m}, 0.088\ \text{m})$; dashed-dotted, $(x_s, r_s) =$

$(2.06\ \text{m}, 0.052\ \text{m})$; dotted, $(x_s, r_s) = (1.56\ \text{m}, 0.088\ \text{m})$. Wide band analysis of 500 Hz bandwidth.

Figure 13. Level (dB) of the MaxSNR beamforming output for different steering positions. Five configurations with a flow rate of 140 l/s: (a), background noise only; (b), source at $(x_s, r_s) = (0.56\ \text{m}, 0.052\ \text{m})$; (c), source at $(x_s, r_s) = (0.56\ \text{m}, 0.088\ \text{m})$; (d), source at,$(x_s, r_s) = (2.06\ \text{m}, 0.052\ \text{m})$; (e), source at $(x_s, r_s) = (1.56\ \text{m}, 0.088\ \text{m})$. Results for the band [4.5 kHz-5 kHz]. Position of the source symbolized by a black disk. Unavailable position symbolized by a white cross.

Table caption

Table 2. Summary of the devices used for the signal processing.

Table 2. Gain values for resonance frequencies identified in figure 4a. Case of an acoustic source at $(x_s, r_s, \theta_s) = (0.56\ \text{m}, 0.052\ \text{m}, 0°)$ and for a flow rate of 140 l/s. Bold values indicate local peaks on the gain curve.

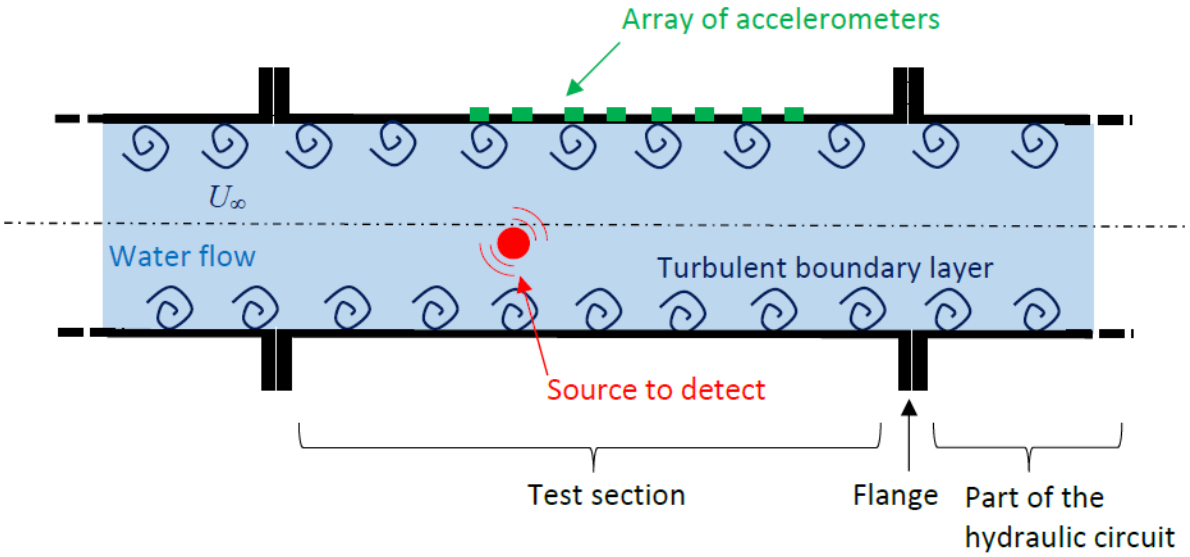

Figure 1. Schematic representation of the configuration considered for assessing the performance of the vibroacoustic beamforming.

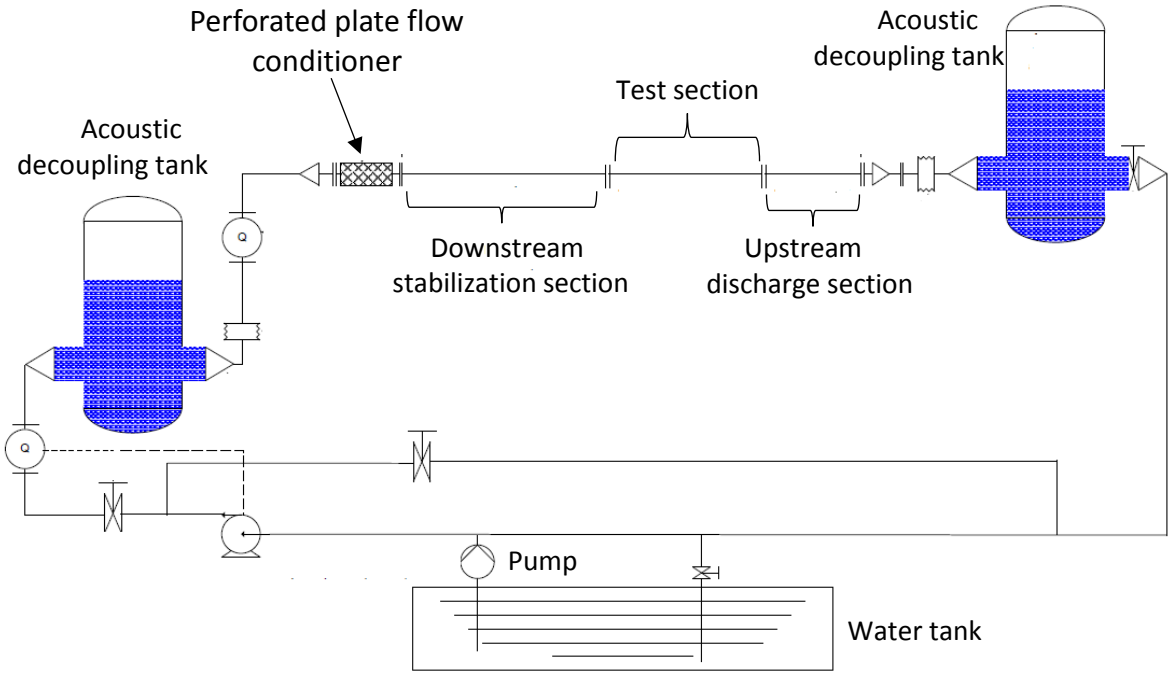

(a)

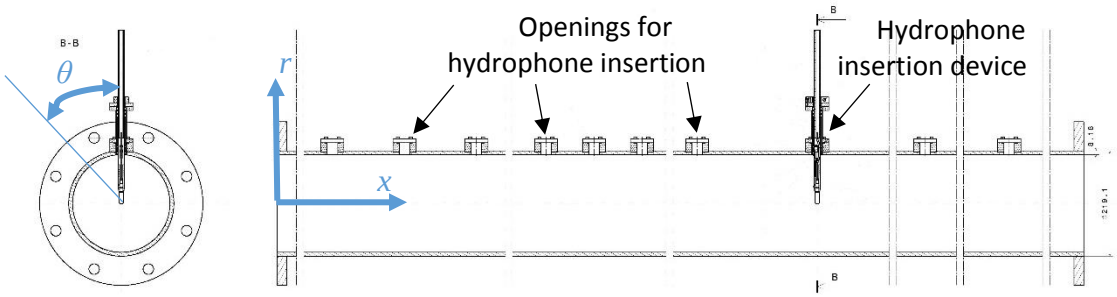

(b)

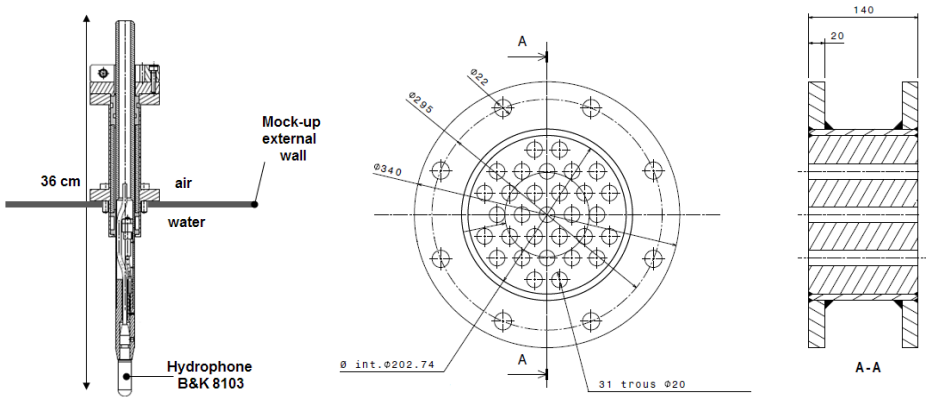

(c)

Figure 2. Experimental setup diagrams: (a), pipe test section inserted in the hydraulic loop; (b), pipe test section with various holes for inserting the hydrophone; (c), hydrophone mounting system (left) and perforated plate conditioner (right).

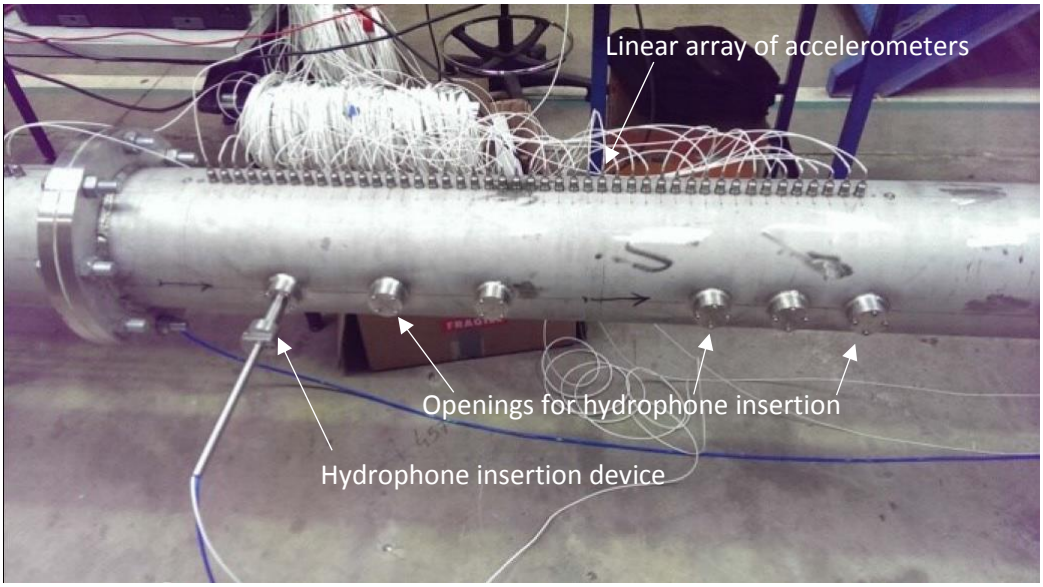

Figure 3. Picture of the test pipe with the linear array of accelerometers.

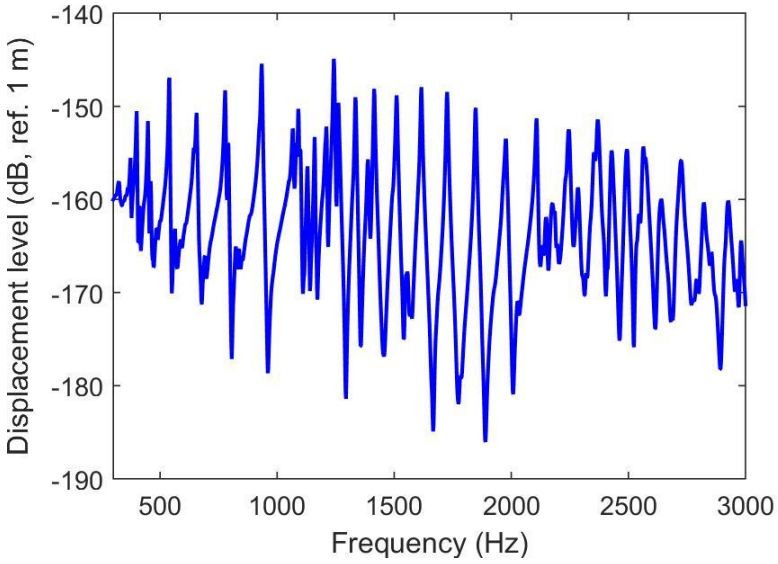

(a)

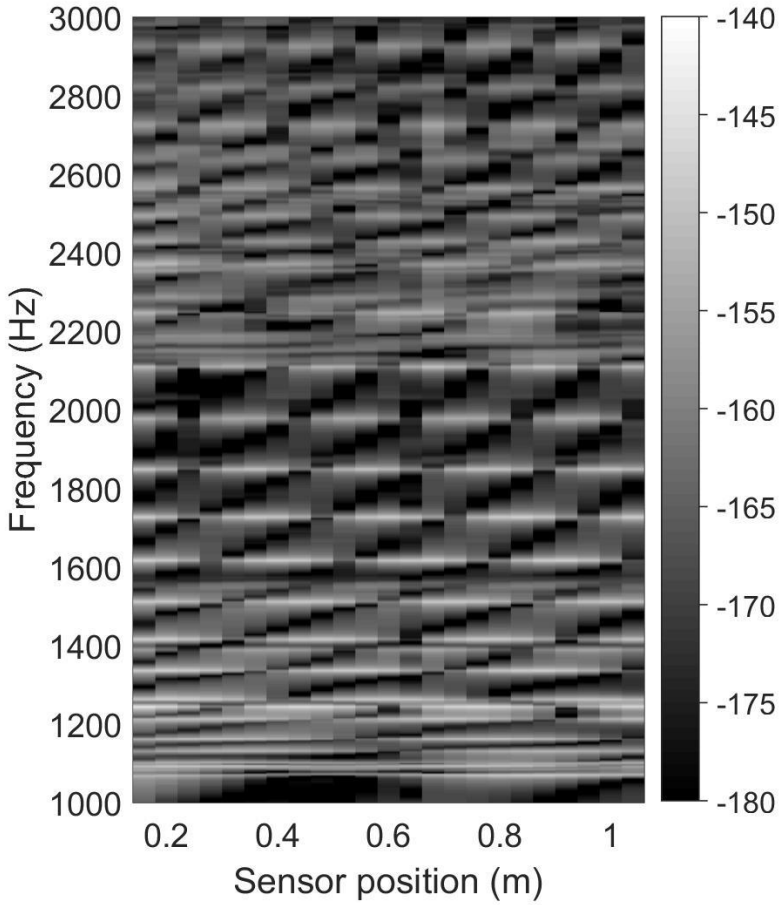

(b)

Figure 4. Radial displacement response of the test pipe for a unit radial mechanical point force at x=0.105 m (hammer excitation): (a), Frequency Response Function (FRF) at point x=1 m (i.e. sensor #21); (b), Displacement versus sensor position and frequency (dB, ref. 1 m).

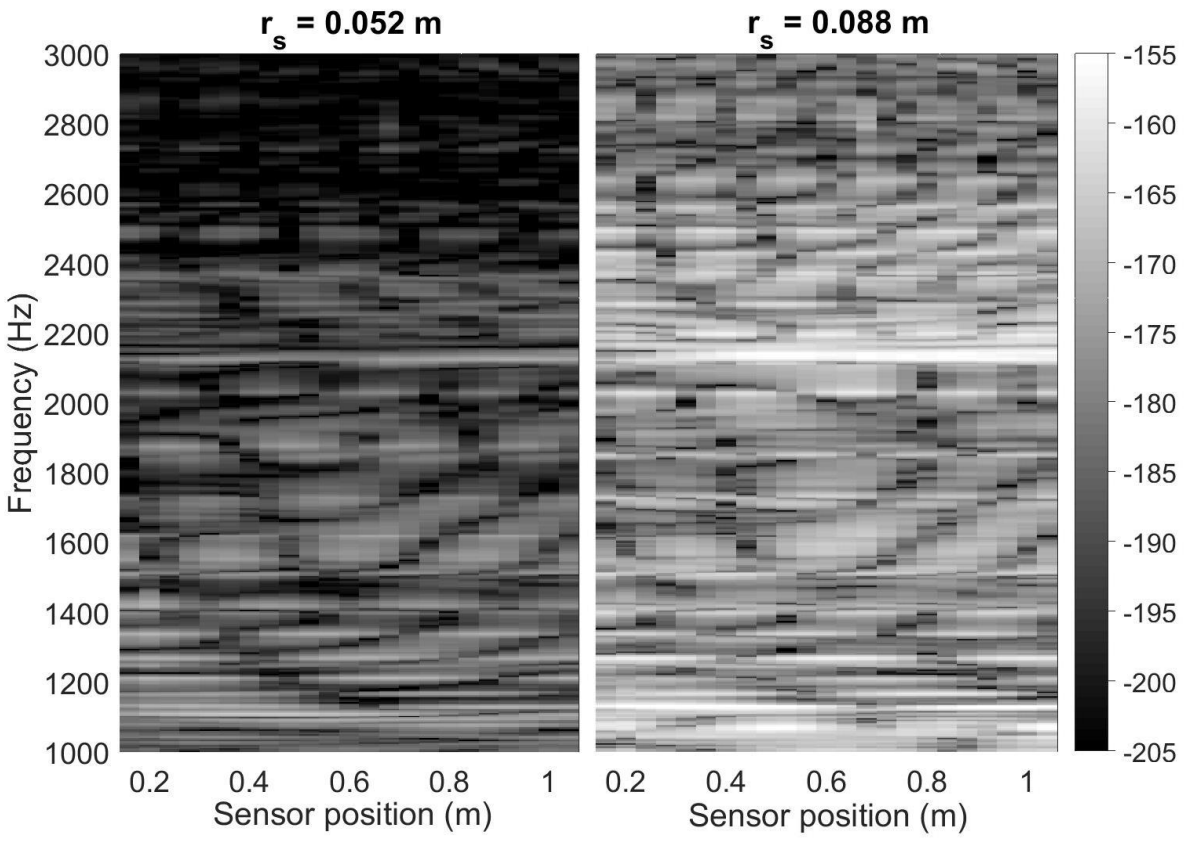

(a) (b)

Figure 5. Radial displacement response as a function of the sensor position and the frequency (dB, ref. 1 m) for an acoustic source excitation (i.e. hydrophone emitter) at two positions: (a), $(x_s, r_s, \theta_s) = (0.56\ \text{m}, 0.052\ \text{m}, 0°)$; (b), $(x_s, r_s, \theta_s) = (0.56\ \text{m}, 0.088\ \text{m}, 0°)$.

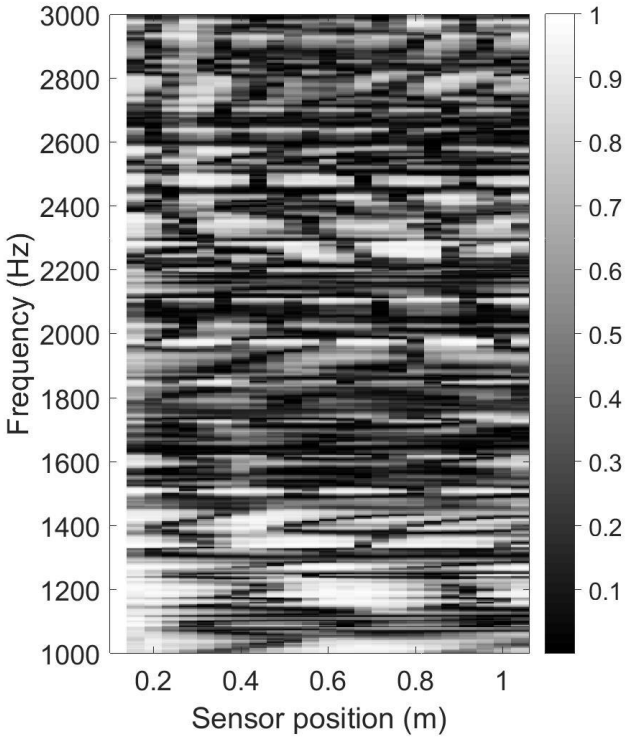

Figure 6. Normalized cross spectrum density function between sensor #1 and sensor #*i*. Results as a function of the position of sensor #*i* and the frequency for a flow rate of 140 l/s.

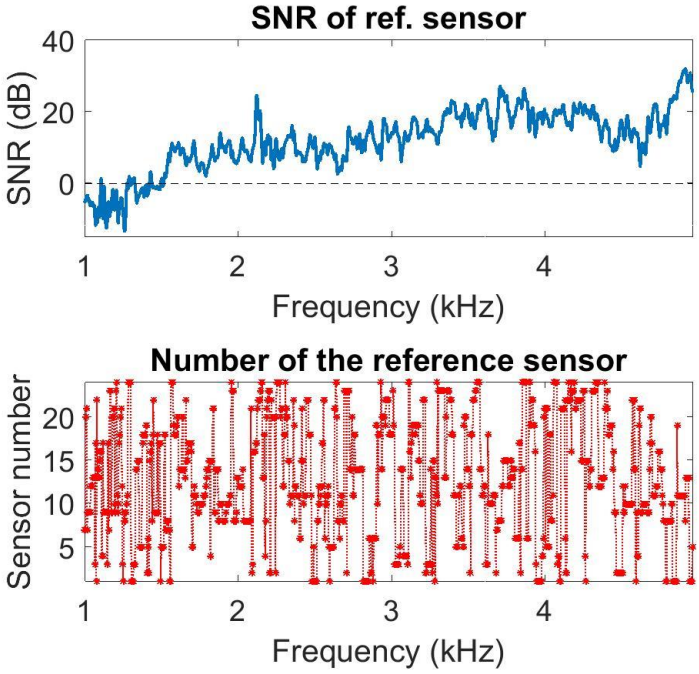

(a)

(b)

Figure 7. (a) Signal to noise ratio for the reference sensor. (b) Identification number of the reference sensor for each frequency. Case of an acoustic source at $(x_s, r_s, \theta_s) = (0.56\ \text{m}, 0.052\ \text{m}, 0°)$ and for a flow rate of 140 l/s.

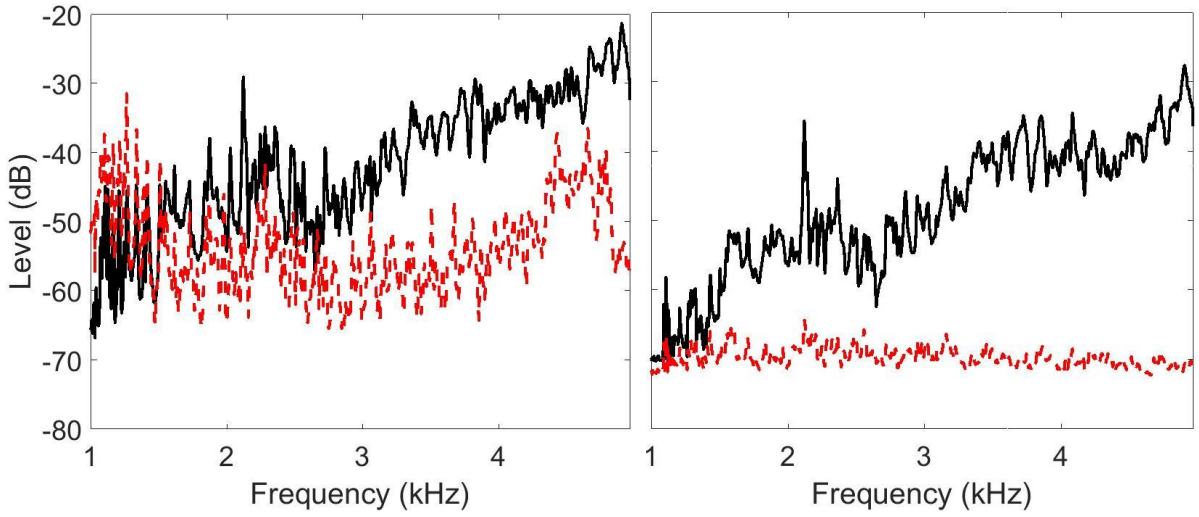

(a) (b)

Figure 8. Output levels of the beamforming, focusing on the source in the presence of the source only (full) and for the noise only (dash): (a), Conventional BF; (b), MaxSNR BF. Case of an acoustic source at $(x_s, r_s, \theta_s) = (0.56\ \text{m}, 0.052\ \text{m}, 0°)$ and for a flow rate of 140 l/s.

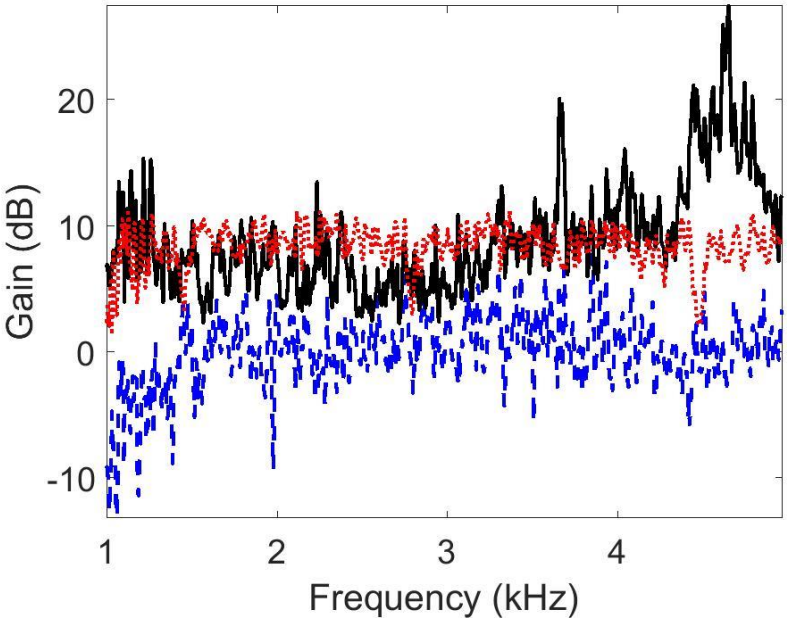

Figure 9. Array gain as a function of frequency: full, MaxSNR BF; dashed, conventional BF; dashed; dotted, theoretical values for the conventional BF supposing uncorrelated noise. Case of an acoustic source at $(x_s, r_s, \theta_s) = (0.56\ \text{m}, 0.052\ \text{m}, 0°)$ and for a flow rate of 140 l/s.

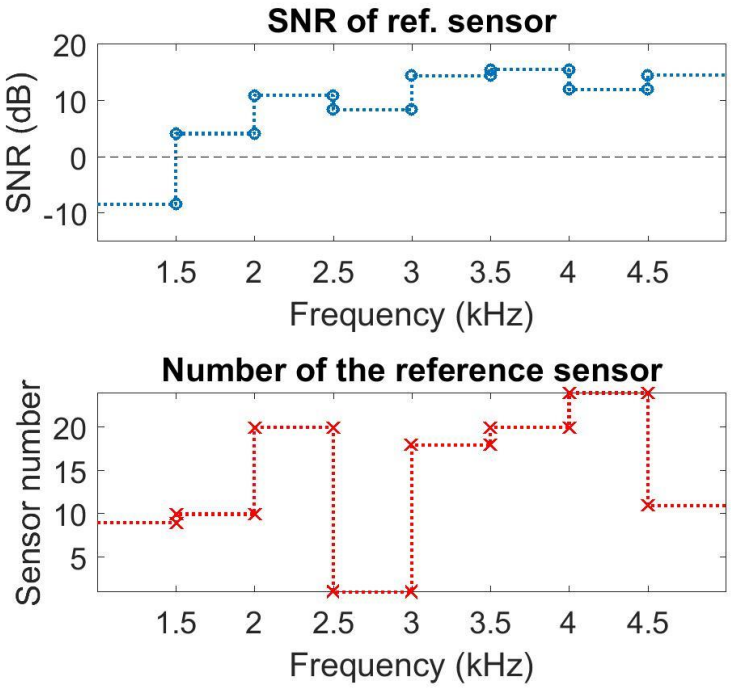

(a)

(b)

Figure 10. As for figure 7 for a wide band analysis of 500 Hz bandwidth.

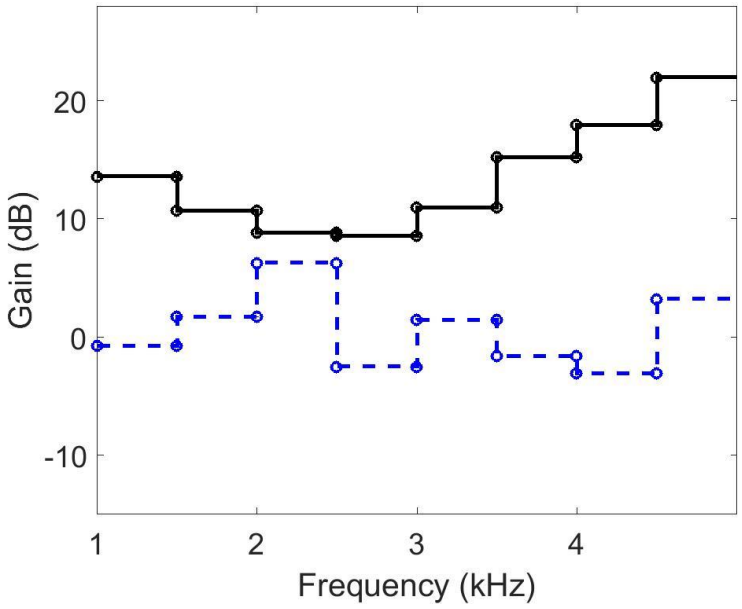

Figure 11. As for figure 9 for a wide band analysis of 500 Hz bandwidth.

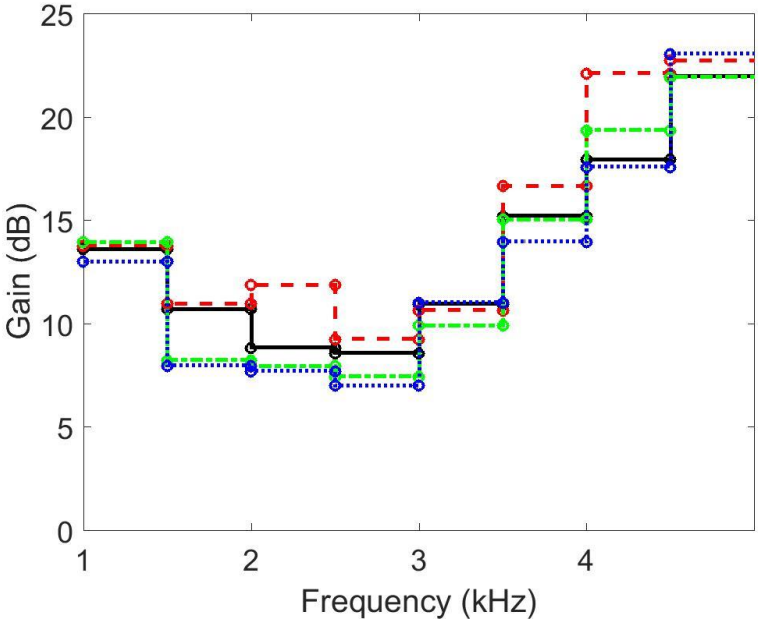

Figure 12. Gain with the MaxSNR beamforming for different source positions: full, $(x_s, r_s) = (0.56\text{ m}, 0.052\text{ m})$; dash, $(x_s, r_s) = (0.56\text{ m}, 0.088\text{ m})$; dashed-dotted, $(x_s, r_s) = (2.06\text{ m}, 0.052\text{ m})$; dotted, $(x_s, r_s) = (1.56\text{ m}, 0.088\text{ m})$. Wide band analysis of 500 Hz bandwidth.

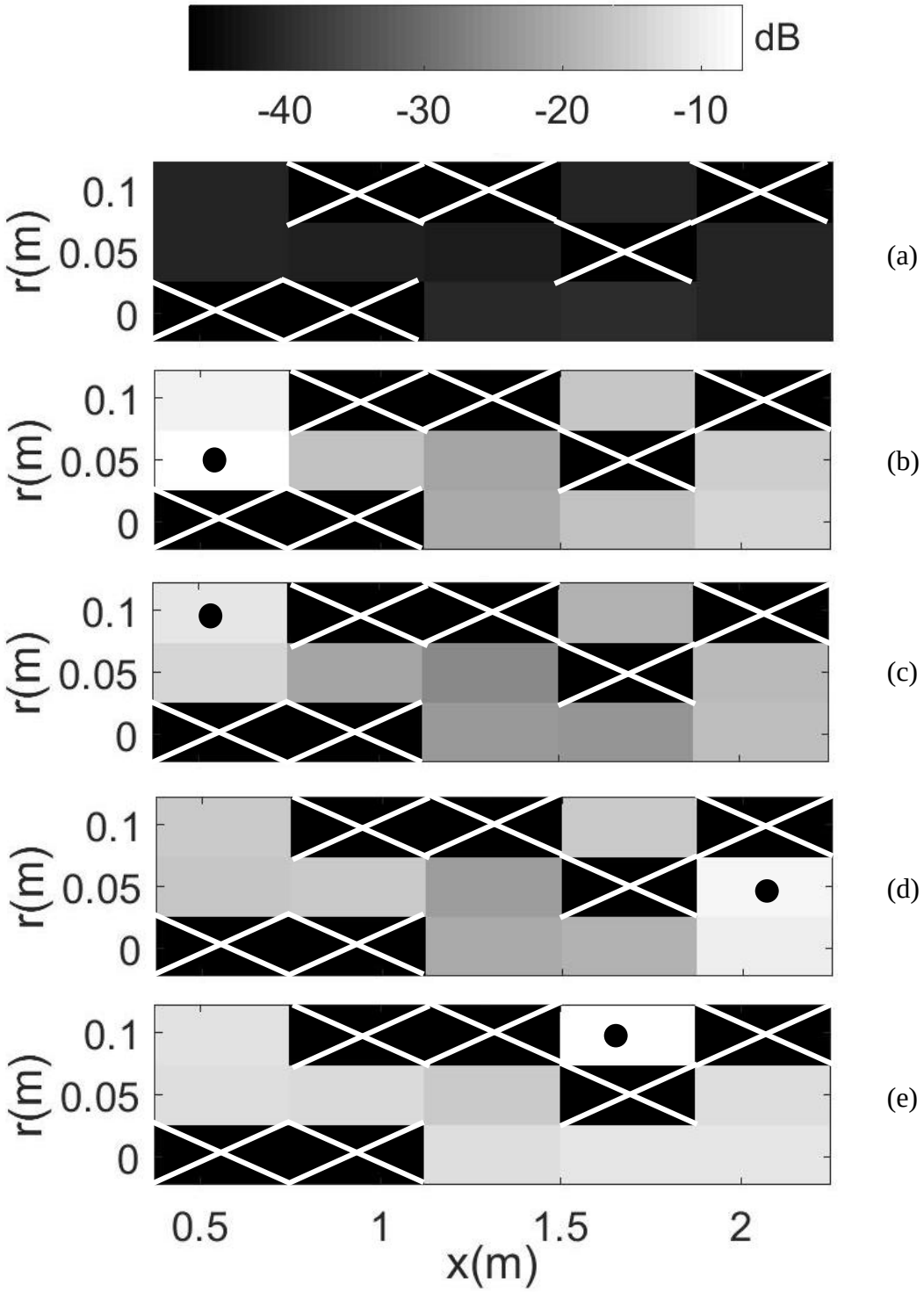

Figure 13. Level (dB) of the MaxSNR beamforming output for different steering positions. Five configurations with a flow rate of 140 l/s: (a), background noise only; (b), source at $(x_s, r_s) = (0.56\ \text{m}, 0.052\ \text{m})$; (c), source at $(x_s, r_s) = (0.56\ \text{m}, 0.088\ \text{m})$; (d), source at,$(x_s, r_s) = (2.06\ \text{m}, 0.052\ \text{m})$; (e), source at $(x_s, r_s) = (1.56\ \text{m}, 0.088\ \text{m})$. Results for the band [4.5 kHz-5 kHz]. Position of the source symbolized by a black disk. Unavailable position symbolized by a white cross.